

Supplementary Information for

***Eco-friendly CoFe₂O₄ Ferrite Nanoparticles Prepared Using
Greek Yogurt solution: Deep Insights Into Optical Properties and
Abnormal Semiconductor-Insulator-Semiconductor Transitions
for Optoelectronics and Catalytic Applications***

Heba Hussein*, S. S. Ibrahim, Sherif A. Khairy
Physics Department, Faculty of Science, Cairo University, Cairo-11566, Egypt

*Corresponding author, Email: Heba@sci.cu.edu.eg

Experimental work

Analysis and Characterization

a) X-ray diffraction (XRD) analysis

The crystal structure of the synthesized CoFe_2O_4 ferrite nanoparticles was characterized using an X'Pert PRO-PANalytical X-ray diffractometer. The XRD measurements were conducted employing a Cu-K_α radiation source ($\lambda = 1.5406 \text{ \AA}$) with a secondary monochromator Holland radiation and a tube voltage of 45 kV. Data collection was performed at room temperature, spanning a 2θ range from 16° to 80° . The Rietveld profile analysis of the sample's crystal structure and microstructure was carried out using FullProf.2k software (version 7.95 - Jan2023 - ILL-JRC). (Angular Resolution Approximately $0.002^\circ 2\theta$, Goniometer Accuracy: $\pm 0.0025^\circ$, Goniometer Reproducibility: $\pm 0.0001^\circ$, Minimum Step Size: 0.0001° , and Measurement Range: $3^\circ < 2\theta \leq 135^\circ$)

b) UV-VIS-NIR spectroscopy Measurement

The optical properties of the synthesized CoFe_2O_4 sample were analyzed using a Jasco-V-770 UV-Vis-NIR spectrophotometer (Japan), which was equipped with an integrating sphere reflectance unit (ISN), covering a wavelength range of 190 to 2000 nm. (Wavelength Range: 190 to 2,700 nm-extendable to 3,200 nm), Wavelength Accuracy: $\pm 0.3 \text{ nm}$ at 656.1 nm; $\pm 1.5 \text{ nm}$ at 1,312.2 nm, Wavelength Repeatability: $\pm 0.05 \text{ nm}$ (UV-Vis); $\pm 0.2 \text{ nm}$ (NIR), Spectral Bandwidth: Variable; UV-Vis: 0.1 to 10 nm; NIR: 0.4 to 40 nm, Photometric Accuracy: $\pm 0.0015 \text{ Abs}$ (0 to 0.5 Abs); $\pm 0.0025 \text{ Abs}$ (0.5 to 1 Abs), Photometric Range: UV-Vis: -4 to 4 Abs; NIR: -3 to 3 Abs, and RMS Noise: 0.00003 Abs)

c) Dielectric measurement

The dielectric properties were measured using a HIOKI 3532-50 LCR high-frequency range tester, operating within a frequency range of 100 Hz to 1 MHz. The measurements were conducted over a temperature range from 303 K to 493 K. The CoFe_2O_4 nanoparticles were formed into pellets with a diameter of 1.2 cm and a thickness of approximately 1.8 mm. (Frequency Range: 42 Hz to 5 MHz), Measurement Time: Minimum of 5 ms, Measurement Parameters: Fourteen, including DC resistance, Measurement Resolution and Accuracy: High resolution and accuracy, though specific values are not detailed in the provided source)

d) Brunauer-Emmett-Teller (BET) analysis

Nitrogen adsorption and desorption isotherms at 77 K were utilized to evaluate the specific surface area and pore size using the multipoint BET method on a Quantachrome analyzer Nova 2000 series instrument (USA).

e) Catalytic activity

A 30% w/w concentration of hydrogen peroxide has been procured from Sigma Aldrich. Catalytic decomposition studies have been conducted at room temperature under continuous stirring at 800 rpm (mechanical stirring). The catalyst dosage employed was 0.75 g/L, and the initial hydrogen peroxide concentration was set at 120 mM. Following a specified duration, the catalyst was separated from the solution using a magnet. The remaining hydrogen peroxide concentration was assessed through spectrophotometry at 240 nm using a Shimadzu 2401 UV-Vis spectrometer. (Wavelength Range: 190 to 900 nm, Wavelength Accuracy: $\pm 0.3 \text{ nm}$, Spectral Bandwidth: Variable, with a minimum of 0.1 nm, and Photometric Accuracy: $\pm 0.002 \text{ Abs}$ (0 to 0.5 Abs))

Structural properties

X-Ray diffraction

Table S1: Lattice constant (a), angle (α , β , and γ), unit cell volume (V), and the agreement factors (R_B %), (R_F %), (R_w), (R_{exp}), (GOF) and (χ^2) of the Rietveld structure refinement of the cobalt ferrite nanoparticle [1]

Parameters	Values
Crystal structure	Cubic
Space group	Fd3m
a (Å)/ b (Å)/ c (Å)	8.371
V(Å) ³	586.530
$\alpha^\circ / \beta^\circ / \gamma^\circ$	90
X-Ray density, ρ_X (g/cm ³)	5.279
Bulk Density, ρ_B (g/cm ³)	3.892
Porosity %, (P_o %)	26.281
R_B (%)	3.73
R_F (%)	3.37
R_{exp}	21.62
R_w	21.70
GOF	1.00
χ^2	1.00
Cation distribution	(Co _{0.255} Fe _{0.745})A(Co _{0.745} Fe _{1.255})B

The values of hopping lengths, L_A , L_B , and L_{AB} for the spinel structure are provided by the following formulas [2,3]:

$$L_A = \left(\frac{a}{4}\right)\sqrt{3} \quad S1$$

$$L_B = \left(\frac{a}{4}\right)\sqrt{2} \quad S2$$

$$L_{AB} = \left(\frac{a}{8}\right)\sqrt{11} \quad S3$$

The hopping lengths are advocated by the polaron radius, which is given by the following equation [4]:

$$\gamma_p = \frac{1}{2} \sqrt[3]{\frac{\pi a^3}{576}} \quad S4$$

The following formula [5] can be used to predict the ionic packing coefficients P_a and P_b at tetrahedral and octahedral sites, respectively:

$$P_a = \frac{d_{AL} - R_o}{r_A} \quad S5$$

$$P_b = \frac{d_{BL} - R_o}{r_B} \quad S6$$

where d_{AL} , d_{BL} , r_A , r_B , and R_o are the average bond length at the tetrahedral and octahedral sites, the mean ionic radii at tetrahedral and octahedral respectively, and R_o is the ionic radius of the oxygen anion, the values of these parameters were obtained from our earlier work [1].

The fulfilment coefficient of the unit cell, (α_V), can be given as [6]:

$$\alpha_V = \frac{32\pi(r_A^3 + 2r_B^3 + 4R_o^3)}{3a_{exp}^3} \quad S7$$

where a_{exp} denotes the experimental lattice constant.

The vacancy parameter β_V [6]. It can be calculated using the following equation [5,6]:

$$\beta_V = \frac{a_{th}^3 - a_{exp}^3}{a_{th}^3} \times 100 \quad S8$$

where a_{th} and a_{exp} are the theoretical and experimental lattice constants.

Table S2: Hopping lengths (L_A), (L_B), (L_{AB}), ionic packing coefficients at tetrahedral and octahedral sites (P_a), (P_b), fulfillment coefficients (α_V), and vacancy parameter (β_V) for the green synthesized cobalt ferrite nanoparticles

Distance between cations at tetrahedral site, L_A (Å)	3.625
Distance between cations at octahedral site, L_B (Å)	2.960
Distance between cations at tetrahedral and octahedral site, L_{AB} (Å)	3.470
Polaron radius, γ_p (Å)	0.737
Vacancy Model Parameters	
Ionic packing coefficients at tetrahedral, P_a	0.979
Ionic packing coefficients at octahedral, P_b	0.987
Fulfillment coefficient, α_V	0.644
Vacancy parameter, β_V (%)	1.49

Optical properties

The Kubelka–Munk function ($F(R)$) is given by the following equation [7]:

$$F(R) = \frac{\alpha}{S} = \frac{(1-R)^2}{2R} \quad S9$$

where R represents diffuse reflectance, α is the absorption coefficient, S is the scattering factor, and $F(R)$ is the Kubelka–Munk function.

The following relation [8] is used to estimate the value of the absorption coefficient α :

$$\alpha = \frac{4\pi K}{\lambda} \quad S10$$

where K and λ stand for extinction coefficient and wavelength of incoming light, respectively.

The absorption spectra can be used to determine Urbach energy, which can be calculated using the following relation [9].

$$\alpha = \alpha_0 \exp\left(\frac{E}{E_u}\right) \quad S11$$

$$\ln\alpha = \ln\alpha_0 + \frac{E}{E_u} \quad S12$$

where E represents the incident photon energy ($h\nu$), α represents the absorption coefficient, and α_0 is constant.

The steepness parameter $S(T)$ can be estimated using the following relation [10]:

$$E_u = \frac{k_B T}{S(T)} \quad S13$$

where T represents room temperature, and k_B is the Boltzmann constant. The steepness parameter $S(T)$ is a physical characteristic of the band gap, indicating how the absorption edge broadens due to interactions between excitons or electrons and phonons [11].

The steepness parameter can be given in terms of electron-phonon interaction E_{e-ph} [11]:

$$E_{e-ph} = \frac{2}{3S} \quad S14$$

The value of the maximum wavelength (λ_T) of the incident light can be calculated using the following equation ^[12]:

$$\left(\frac{\alpha}{\lambda}\right)^2 = C \left(\frac{1}{\lambda}\right) - \left(\frac{1}{\lambda_T}\right) \quad \text{S15}$$

here C is a constant.

The calculation of the penetration depth (δ) is based on the relationship that defines the $\alpha(\lambda)$ curve, as follows ^[13]:

$$\delta = \frac{1}{\alpha(\lambda)} \quad \text{S16}$$

The extinction coefficient k can be calculated using the following formula ^[14]:

$$k = \frac{\alpha\lambda}{4\pi} \quad \text{S17}$$

The refractive index n can be determined using the following relationship ^[15]:

$$n(\lambda) = \frac{1+R}{1-R} - \sqrt{\left(\frac{4R}{(1-R)^2} - k^2\right)} \quad \text{S18}$$

where k is the extinction coefficient and R is the reflection.

The Cauchy parameters n_0 , n_1 , and n_2 can be employed, as detailed in the following equation ^[16]:

$$n = n_0 + \frac{n_1}{\lambda^2} + \frac{n_2}{\lambda^4} \quad \text{S19}$$

Wemple-DiDomenico relationship was expressed as follows ^[17] to determine the dispersion energy E_d and the energy of the effective single oscillator E_0 .

$$n^2 - 1 = \frac{E_0 E_d}{E_0^2 - (h\nu)^2} \quad \text{S20}$$

The static refractive index n'_0 and the optical dielectric constant ϵ_{op} at zero frequency can be estimated using the following equation:

$$\epsilon_{op} = n_0'^2 = 1 + \frac{E_d}{E_0} \quad \text{S21}$$

The average oscillator wavelength λ_0 and oscillator strength S_0 can be given by the following relationship ^[18]:

$$\frac{1}{n^2 - 1} = \frac{1}{S_0 \lambda_0^2} - \frac{1}{S_0 \lambda^2} \quad \text{S22}$$

The moments of the optical spectrum M_{-1} and M_{-3} were calculated using the following relationships ^[19]:

$$E_0^2 = \frac{M_{-1}}{M_{-3}} \quad \text{S23}$$

$$E_d^2 = \frac{M_{-1}^3}{M_{-3}} \quad \text{S24}$$

Table S3: Summarized optical parameters of the eco-friendly synthesized CoFe₂O₄ nanoparticles

Parameters	Values
DSR method	
E _g (direct) (eV)	1.460 ^[1]
E _g (indirect) (eV)	0.800
E _u (eV)	0.360
E _{e-ph} (eV)	10
S	0.067
Cauchy's parameters	
n ₀	1.800
n ₁ (μm ²)	0.016
n ₂ (μm ⁴)	9.660 × 10 ⁻⁴
Wemple DiDomenico model (WDD)	
E ₀ (eV)	1.16 0
E _d (eV)	3.08 0
S ₀ (nm ⁻²)	3.64×10 ⁻⁴
λ ₀ (nm)	1174.620
M ₋₁	2.660
M ₋₃ (eV ⁻²)	1.990
Mullikan electronegativity method	
E _{CB} (eV)	0.580 ^[1]
E _{VB} (eV)	2.040 ^[1]

The optical conductivity (σ_{op}) for the prepared cobalt ferrite sample as a function of wavelength (λ) can be given by the following equation ^[20]:

$$\sigma_{OP} = \frac{\alpha n c}{4\pi K} \quad \text{S25}$$

In this equation, C represents the speed of light.

The complex dielectric permittivity was given by the following relation ^[21]:

$$\varepsilon(\lambda) = [n(\lambda) - iK(\lambda)]^2 = \varepsilon_1(\lambda) - i\varepsilon_2(\lambda) \quad \text{S26}$$

The real ε₁ and imaginary ε₂ are components of the optical dielectric permittivity, which can be expressed as follows:

$$\varepsilon_1(\lambda) = n^2(\lambda) - k^2(\lambda) \quad \text{S27}$$

$$\varepsilon_2(\lambda) = 2n(\lambda) k(\lambda) \quad \text{S28}$$

The band edges of the conduction band (CB) and valence band (VB) can be estimated utilising the Mulliken electronegativity rules concerning the normal hydrogen electrode (NHE) scale at pH=0, using the following relations ^[22]:

$$E_{CB} = \chi - E^e - 0.5E_g \quad \text{S29}$$

$$E_{VB} = E_{CB} + E_g \quad \text{S30}$$

where the conduction band edge is represented by E_{CB}, the optical energy band gap between the sample's VB and CB by E_g, and the valence band edge by E_{VB}. E^e refers to free electron energy, which is 4.5 eV on the hydrogen scale.

The absolute electronegativity of the prepared CoFe₂O₄ sample, also known as Mullikan electronegativity (χ), can be calculated using the following equation ^[23]:

$$\chi = [\chi(A)^a \chi(B)^b \chi(C)^c]^{\frac{1}{(a+b+c)}} \quad \text{S31}$$

The above equation incorporates the number of atoms in the molecule, denoted by the variables a, b, and c. The χ (A) value is calculated by averaging the electron affinity and initial ionisation energy for atom A. Calculations were carried out to estimate χ (B) and χ (C).

Electrical properties (Dielectric measurements)

AC conductivity

The AC conductivity at various frequencies and temperatures can be calculated using the following formula ^[24] which is derived from dielectric data:

$$\sigma_{ac} = \omega \epsilon_0 \epsilon_r \tan \delta \quad \text{S32}$$

In the above equation, ϵ_0 represents the permittivity of vacuum and ϵ_r refers to the relative dielectric constant.

The universal Jonscher's power law is given by the following equation ^[25,26]:

$$\sigma_T(\omega) = \sigma_{dc} + \sigma_{ac}(\omega) = \sigma_{dc} + A(T)\omega^{s(T)} \quad \text{S33}$$

In this equation, $\sigma_T(\omega)$ represents the total conductivity, where σ_{dc} is the frequency-independent DC conductivity, and $\sigma_{ac}(\omega)$ is the purely dispersive AC component.

The frequency exponent s is mathematically expressed within the CBH model using the following equation ^[27], reflecting the nature of the hopping mechanism and charge transport across the material.

$$s = 1 - \frac{6kT}{W_M - kT \ln(\omega \tau_0)} \quad \text{S34}$$

In the above equation, T represents the temperature, k is the Boltzmann constant, ω is the angular frequency, τ_0 denotes the relaxation time, and W_M is the maximum barrier height. For high values of W_M/kT , the variable s simplifies to the following form ^[28]:

$$s = 1 - \frac{6kT}{W_M} \quad \text{S35}$$

The Arrhenius relation is given as ^[29]:

$$\sigma_{dc} = \frac{\sigma_0}{T} \exp\left(\frac{E_a}{kT}\right) \quad \text{S36}$$

In this context, σ_0 , k , and E_a represent the pre-exponential factor, the Boltzmann constant, and the activation energy, respectively.

Table S4: Fitting parameters were determined using Jonscher's power, double Jonscher's power, and super linear power laws based on the experimental data of AC conductivity as a function of frequency at various temperatures

JPL								
Temperature	σ_{dc} (s/m)	A	s	R ²				
303	1.0E-5	6.230E-5	0.101	0.9987				
308	1.5E-5	1.196E-4	0.094	0.9922				
313	2.0E-5	1.850E-4	0.088	0.9914				
318	3.5E-5	2.960E-4	0.083	0.9915				
323	6.0E-5	8.750E-4	0.077	0.9785				
328	1.4E-4	1.100E-3	0.072	0.9724				
333	3.0E-4	1.300E-3	0.068	0.9601				
DJPL								
Temperature	σ_{dc} (s/m)	A1	s1	A2	s2	R ²		
343	6.051E-5	8.991E-9	0.530	9.250E-9	0.530	0.9991		
348	2.816E-5	8.00E-9	0.530	7.579E-9	0.530	0.9968		
353	1.859E-5	6.604E-9	0.530	7.325E-9	0.530	0.9992		
DJPL						SLP		
Temperature	σ_{dc} (s/m)	A1	s1	A2	s2	B3	s3	R ²
358	1.381E-5	6.472E-9	0.530	7.311E-9	0.530	2.216E-19	1.2	0.9996
363	1.176E-5	6.600E-9	0.530	7.420E-9	0.530	3.000E-19	1.2	0.9994
368	1.049E-5	6.892E-9	0.530	7.679E-9	0.530	3.500E-19	1.2	0.9992
373	8.991E-6	7.522E-9	0.530	8.039E-9	0.530	4.000E-19	1.2	0.9993
DJPL								
Temperature	σ_{dc} (s/m)	A1	s1	A2	s2	R ²		
383	3.615E-7	2.368E-8	0.5190	8.101E-9	0.0004	0.9989		
393	8.632E-7	1.433E-8	0.5597	8.995E-6	0.0029	0.9989		
403	2.058E-6	9.986E-9	0.591	9.614E-6	0.0050	0.9985		
413	4.562E-6	8.889E-9	0.618	1.566E-5	0.0070	0.9979		
423	1.000E-5	5.426E-9	0.649	1.62E-5	0.0093	0.9550		
433	1.463E-5	3.577E-9	0.682	2.275E-5	0.0114	0.9978		
443	2.611E-5	2.332E-9	0.714	2.575E-5	0.0135	0.9985		
453	3.971E-5	1.509E-9	0.746	2.705E-5	0.016	0.9995		
463	7.114E-5	9.977E-10	0.777	2.905E-5	0.018	0.9996		
473	9.217E-5	6.433E-10	0.807	3.236E-5	0.020	0.9997		
483	1.411E-4	4.039E-10	0.840	3.536E-5	0.022	0.9976		
493	2.260E-4	2.149E-10	0.880	3.736E-5	0.024	0.9977		

The alternating current (AC) conductivity for CBH was expressed as ^[30]:

$$\sigma_{ac} = \frac{n}{24} \pi^2 NN_p \epsilon' \omega R_\omega \quad S37$$

In this model, n represents the number of polarons involved in the hopping process. During the procedure (with n = 1 or n = 2), the dielectric constant is assumed to be ϵ' for the prepared sample. The term NN_p is proportional to the square of the concentration of states, while R_ω denotes the hopping distance under the condition of $\omega\tau=1$ and is defined by the following equation:

$$R_\omega = \frac{e^2}{\pi \epsilon' \epsilon_0 \left(W_M - k_B T \ln \left(\frac{1}{\omega \tau_0} \right) \right)} \quad S38$$

where τ_0 is the relaxation time and it can be given as, $\tau_0 = 1/2\pi f_0$ where $f_0 = 10^{13}$ Hz ^[31,32].

The double Jonscher power law (DJPL) can be analyzed using the Bruce model. ^[33,34], which can be expressed as follows:

$$\sigma_T(\omega) = DJPL = \sigma_{dc} + A1(T)\omega^{s1(T)} + A2(T)\omega^{s2(T)} \quad S39$$

In this context, A1 and A2 represent two temperature-dependent variables, which determine the polarizability's strength, while the parameters s1 and s2 are frequency exponents that vary with temperature. These parameters describe the behavior of the system in response to different frequencies at different temperatures, allowing for a more detailed understanding of the material's conductivity characteristics.

According to the QMT conduction mechanism, the AC conductivity can be given as follows [35]:

$$\sigma_{ac} = A e^2 k_B T \alpha^{-1} (N(E_F))^2 \omega R_\omega^4 \quad S40$$

In the above equation, A represents a constant $= \frac{\pi^4}{24}$ [36] or $= \frac{\pi^2}{12}$ [30], k represents Boltzmann constant, e is the charge of electron, $N(E_F)$ is the density of state near the fermi level, and R_ω is the tunneling distance a certain angular frequency ω

According to the quantum mechanical tunneling model (QMT), the tunneling distance R_ω can be given as :

$$R_\omega = \frac{1}{2\alpha} \text{Ln} \left(\frac{1}{\omega\tau_0} \right) \quad S41$$

The spatial decay parameter ($\alpha^{-1} = 10 \text{ \AA}$) [37] represents the rate at which the wave function decreases, reflecting the localized nature of the state at each position. This parameter indicates how quickly the probability of finding an electron diminishes as the distance from a localized center increases.

The exponent s can be determined using the NSPT model through the following equation [38]:

$$s = 1 + \frac{4k_B T}{W_m - k_B T \text{Ln}(\omega\tau_0)} \quad S42,$$

where W_m represents the carrier's binding energy at its localized sites and k_B is the Boltzmann constant.

For large $W_m/k_B T$ ratios, the parameter s is given by:

$$s = 1 + \frac{4k_B T}{W_m} \quad S43$$

Based on the NSPT model, the AC conductivity can be described by the following equation [39]:

$$\sigma_{ac} = \frac{(\pi e)^2 k_B T \alpha^{-1} (N(E_F))^2 \omega R_\omega^4}{12} \quad S44$$

where

$$R_\omega = \frac{1}{2\alpha} \left(\text{Ln} \left(\frac{1}{\omega\tau_0} \right) - \frac{W_h}{k_B T} \right) \quad S45$$

In this context, the tunnelling distance is denoted as R_ω , the polaron hopping energy is W_h , the density of states near the Fermi level is $N(E_F)$, and the spatial extension of the polaron is represented as α^{-1} . The values of $N(E_F)$, α , and W_H were adjusted to ensure that the computed σ_{ac} versus T curves matched the experimental data.

Table S5: Parameters utilized for fitting the NSPT model for the AC conductivity of the green-synthesized CoFe_2O_4 nanoparticles

Frequency (kHz)	N_F ($\times 10^{38} \text{ eV}^{-1} \text{ m}^{-1}$)		α (\AA^{-1})		W_h (eV)	
	383-423 K	423-493 K	383-423 K	423-493 K	383-423 K	423-493 K
10	0.527	0.618	0.266	0.171	0.551	0.700
100	0.957	1.336	0.755	0.354	0.393	0.609
1000	1.207	1.533	0.964	0.917	0.345	0.393

The AC conductivity (σ_{ac}) was further examined using the Arrhenius equation [40, 41]:

$$\sigma_{ac} = \sigma_0 \exp \left(-\frac{E_a}{k_B T} \right) \quad S46$$

In this equation, σ_0 denotes the pre-exponential factor.

Table S6: Values of activation energy for the green synthesized CoFe₂O₄ nanoparticles at different applied field frequencies

Frequency (kHz)	E _a (I) (eV) (303-333 K)	E _a (II) (eV) (343-373 K)	E _a (III) (eV)	
			(1) (383-423 K)	(2) (423-493 K)
1	0.864	-0.617	0.313	0.542
10	0.846	-0.538	0.284	0.493
100	0.826	-0.389	0.234	0.454
1000	0.784	-0.254	0.222	0.290

Dielectric properties

Havriliak-Negami (H-N) model ^[42,43] which is given by the following expressions:

$$\varepsilon' = \varepsilon_{\infty} + (\varepsilon_s - \varepsilon_{\infty})r^{\frac{-\beta}{2}} \cos\beta\theta \quad S47$$

$$r = \left[1 + (\omega\tau)^{1-\alpha} \sin\left(\frac{\alpha\pi}{2}\right)\right]^2 + \left[(\omega\tau)^{1-\alpha} \cos\left(\frac{\alpha\pi}{2}\right)\right]^2 \quad S48$$

$$\theta = \arctan\left[\frac{(\omega\tau)^{1-\alpha} \cos\left(\frac{\alpha\pi}{2}\right)}{1 + (\omega\tau)^{1-\alpha} \sin\left(\frac{\alpha\pi}{2}\right)}\right] \quad S49$$

here, ε_s and ε_{∞} represent the static and high-frequency dielectric constants, respectively. The characteristic relaxation time is denoted by τ , while α and β are shape parameters constrained by ($0 \leq \alpha\beta \leq 1$). When α and β are equal to 1, the system exhibits ideal Debye relaxation ^[44]. Conversely, any non-zero values of these parameters indicate a range of relaxation times instead of a single relaxation time ^[44].

Table S7: Havriliak-Negami (H-N) fitting parameter values for the synthesized CoFe₂O₄ nanoparticles

Temperature	ε_s	ε_{∞}	$\nabla\varepsilon$	α	β	τ	R ²
303	2.000	2.048E7	2.048E7	0.430	1.070	4.567	0.999
308	2.500	4.533E7	4.533E7	0.435	1 1.130	3.049	0.999
313	3.000	6.975E7	6.975E7	0.443	1.180	1.972	0.994
318	4.000	8.975E7	8.975E7	0.448	1.190	1.416	0.992
323	4.500	2.136E8	2.136E8	0.455	1.220	0.876	0.993
328	5.000	2.739E8	2.739E8	0.458	1.236	0.771	0.991
333	6.000	2.975E8	2.975E8	0.462	1.246	0.701	0.999
343	2.800	3.606E3	3.603E3	0.465	0.921	0.005	0.996
348	2.500	1.182E3	1.179E3	0.394	0.949	0.006	0.999
353	2.100	1.000E3	0.998E3	0.360	0.964	0.008	0.999
358	1.900	0.934E3	0.932E3	0.340	0.984	0.010	0.996
363	1.700	0.910E3	0.908E3	0.319	1.004	0.012	0.998
368	1.500	0.837E3	0.835E3	0.269	1.104	0.014	0.999
373	1.300	0.732E3	0.730E3	0.230	1.204	0.016	0.999
383	2.000	0.807E3	0.805E3	0.284	0.916	0.025	0.992
393	2.400	0.907E3	0.906E3	0.296	0.920	0.023	0.996
403	2.600	0.997E3	0.994E3	0.300	0.928	0.021	0.997
413	3.600	1.012E3	1.009E3	0.302	0.930	0.019	0.997
423	4.000	1.126E3	1.122E3	0.306	0.931	0.018	0.993
433	4.400	1.229E3	1.225E3	0.307	0.932	0.016	0.991
443	4.600	1.322E3	1.318E3	0.309	0.934	0.014	0.991
453	4.800	1.412E3	1.405E3	0.310	0.941	0.011	0.989
463	5.000	1.708E3	1.703E3	0.315	0.991	0.010	0.989
473	5.100	1.908E3	1.903E3	0.320	0.996	0.009	0.993
483	5.200	2.135E3	2.130E3	0.330	0.999	0.008	0.989
493	5.400	2.292E3	2.287E3	0.340	1.000	0.007	0.992

The Giuntini model ^[45] was employed to analyze the dielectric loss, ε'' as a function of frequency and temperature, using its mathematical expression:

$$\varepsilon''(\omega) = (\varepsilon_0 - \varepsilon_\infty) 2\pi^2 N \left(\frac{ne}{\varepsilon_0}\right)^3 k_B T \tau_0^m W_m^{-4} \omega^m \quad \text{S50}$$

here, ε_0 denotes the static dielectric constant, ε_∞ represents the optical dielectric constant, n is the number of hopping charges, N is the concentration of localized sites, and W_m is the maximum barrier height. Thus, Eq. S50 can be succinctly abbreviated as:

$$\varepsilon''(\omega) = B \omega^m \quad \text{S51}$$

The exponent $m(T)$ may be written as a function of temperature and maximum barrier height W_m according to the following equation:

$$m = \frac{-4kT}{W_M} \quad \text{S52}$$

The dissipation factor, also known as the loss tangent ($\tan \delta$), is defined as the ratio of energy lost or dissipated per cycle to the energy stored and can be represented mathematically as follows:

$$\tan \delta = \frac{\varepsilon''}{\varepsilon'} \quad \text{S53}$$

The condition for observing a peak in the dielectric loss of a dielectric material is defined by the relationship ^[46]:

$$\omega\tau = 1 \quad \text{S54}$$

where τ represents the relaxation time and $\omega = 2\pi f_{\max}$.

Thermodynamic parameters

The relaxation time τ can be calculated using the following relation ^[46]:

$$\tau = \tau_0 \exp\left(\frac{E_d}{kT}\right) \quad \text{S55}$$

here, τ_0 represents the pre-exponential constant, equivalent to the relaxation time at infinitely high temperatures, while k is the Boltzmann constant, T is the temperature in Kelvin, and E_d is the activation energy for dielectric relaxation.

The relaxation time is connected to the free energy through a Eyring hypothesis ^[47]:

$$\tau = \left(\frac{h}{k_B T}\right) \exp\left(\frac{\Delta G}{RT}\right) \quad \text{S56}$$

In this relation, k_B denotes Boltzmann's constant, R represents the gas constant, h is Planck's constant, and ΔG stands for the Gibbs free energy.

The relationship between ΔG , the activation enthalpy ΔH , and the activation entropy ΔS can be expressed by the following equation ^[48]:

$$\Delta G = \Delta H - T\Delta S \quad \text{S57}$$

Thus, the relaxation time can be given as follows:

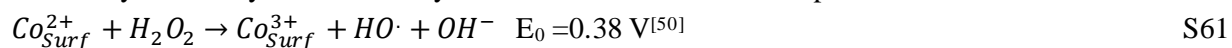
$$\tau = \left(\frac{h}{k_B T}\right) \exp\left(\frac{\Delta H}{RT}\right) \exp\left(\frac{-\Delta S}{R}\right) \quad \text{S58}$$

Catalytic activity of the green-synthesized CoFe₂O₄

The mechanism of H₂O₂ decomposition can be characterized using the following formulas [49]:



The catalytic activity is enhanced by the cobalt ion content in the spinel structure



Co³⁺ ions act as active oxidants and take part in the following reaction [51]:



As a result, Co²⁺ ions are regenerated, and the resulting radicals undergo additional reactions [52]:



Table S8: Performance comparison of the highest catalytic activity for decomposition of H₂O₂ of the present green synthesized CoFe₂O₄ nanoparticles with that of other reported metal oxide catalysts

Catalyst	Reaction Conditions			Rate Constant k (sec ⁻¹)	Ref
	Conc of H ₂ O ₂ (mM)	Dose of catalyst (g/L)	Time (h)		
CoFe ₂ O ₄	100	2	4	1.11×10 ⁻⁴	[135]
CeO ₂	0.5	32	3	1.7 ×10 ⁻⁴	[136]
ZrO ₂	0.5	30	8	6.15×10 ⁻⁴	[137]
CuO	0.5	1.2	3	1.9×10 ⁻⁴	[136]
CoFe ₂ O ₄	120	0.75	2.5	3.39 ×10 ⁻⁴	The present work

References

1. Hussein, H., S. Ibrahim, and S.A. Khairy, *Biosynthesis of CoFe₂O₄ ferrite nanoparticles using Greek yogurt solution: Deep structural insights and appraisal for ecological mitigation via quartz crystal microbalance*. Journal of Water Process Engineering, 2024. **65**: p. 105856.
2. Amer, M., et al., *Mössbauer, Infrared and X-ray Studies for Ni_{0.5}Zn_{0.5}Cr_xFe_{2-x}O₄ Ferrites*. Turkish Journal of Physics, 2005. **29**(3): p. 163-177.
3. Khan, M.Z., et al., *Comprehensive study on structural, electrical, magnetic and photocatalytic degradation properties of Al³⁺ ions substituted nickel ferrites nanoparticles*. Journal of Alloys and Compounds, 2020. **848**: p. 155795.
4. Aslam, A., et al., *Lanthanum doped Zn_{0.5}Co_{0.5}LaxFe_{2-x}O₄ spinel ferrites synthesized via co-precipitation route to evaluate structural, vibrational, electrical, optical, dielectric, and thermoelectric properties*. Journal of Physics and Chemistry of Solids, 2021. **154**: p. 110080.
5. Mohamedda, K., et al., *Infrared and structural studies of Mg-Zn ferrite*. Physica. B, 2012. **407**: p. 795-804.
6. Khalaf, K., et al., *Influence of Zn²⁺ ions on the structural and electrical properties of Mg_{1-x}Zn_xFeCrO₄ spinels*. Journal of Alloys and Compounds, 2016. **657**: p. 733-747.
7. Raddaoui, G., et al., *Investigation studies of structural, electrical, dielectric, and optical of DyTi_{0.5}Mn_{0.5}O₃ multiferroic for optoelectronics applications*. Journal of Materials Science: Materials in Electronics, 2022. **33**(27): p. 21890-21912.
8. Chand, P., S. Vaish, and P. Kumar, *Structural, optical and dielectric properties of transition metal (MFe₂O₄; M= Co, Ni and Zn) nanoferrites*. Physica B: Condensed Matter, 2017. **524**: p. 53-63.
9. Akshay, V., et al., *Visible range optical absorption, Urbach energy estimation and paramagnetic response in Cr-doped TiO₂ nanocrystals derived by a sol-gel method*. Physical Chemistry Chemical Physics, 2019. **21**(24): p. 12991-13004.
10. Husain, S., A.O. Keelani, and W. Khan, *Influence of Mn substitution on morphological, thermal and optical properties of nanocrystalline GdFeO₃ orthoferrite*. Nano-Structures & Nano-Objects, 2018. **15**: p. 17-27.
11. Rejaiba, O., et al., *Investigation study of optical and dielectric parameters using absorption and diffuse reflectance spectroscopy method on La_{0.57}Nd_{0.15}Sr_{0.13}Ag_{0.2}MnO₃ perovskite for optoelectronic application*. Optical and Quantum Electronics, 2022. **54**(5): p. 315.
12. Kharrat, A.B.J., K. Kahouli, and S. Chaabouni, *Detailed investigation of the optical properties of the (C₈H₁₁BrN) ₃BiCl₆ compound by UV-visible measurements*. Bulletin of Materials Science, 2020. **43**(1): p. 275.
13. El Nahrawy, A.M., et al., *Structural and opto-magnetic properties of nickel magnesium copper zircon silicate nano-composite for suppress the spread of foodborne pathogenic bacteria*. Silicon, 2021: p. 1-16.
14. Hemdan, B.A., et al., *Green sol-gel synthesis of novel nanoporous copper aluminosilicate for the eradication of pathogenic microbes in drinking water and wastewater treatment*. Environmental Science and Pollution Research, 2019. **26**: p. 9508-9523.
15. Mansour, A., et al., *Ecofriendly synthesis and characterization of Ni²⁺ codoped silica magnesium zirconium copper nanoceramics for wastewater treatment applications*. Scientific Reports, 2022. **12**(1): p. 9855.
16. Hcini, F., et al., *Structural, optical, and dielectric properties for Mg_{0.6}Cu_{0.2}Ni_{0.2}Cr₂O₄ chromite spinel*. Physica B: Condensed Matter, 2022. **624**: p. 413439.
17. Wemple, S. and M. DiDomenico Jr, *Behavior of the electronic dielectric constant in covalent and ionic materials*. Physical Review B, 1971. **3**(4): p. 1338.
18. Tounsi, N., et al., *Structural and optical characterization of copper oxide composite thin films elaborated by GLAD technique*. Vacuum, 2015. **121**: p. 9-17.
19. Habubi, N., K. Mishjil, and S. Chiad, *Structural properties and refractive index dispersion of cobalt doped SnO₂ thin films*. Indian Journal of Physics, 2013. **87**(3): p. 235-239.

20. Yokokawa, H., et al., *Thermodynamic stabilities of perovskite oxides for electrodes and other electrochemical materials*. Solid State Ionics, 1992. **52**(1-3): p. 43-56.
21. Mguedla, R., et al., *Gd doping effect on structural, electrical and dielectric properties in HoCrO₃ orthochromites for electric applications*. Journal of Alloys and Compounds, 2020. **836**: p. 155186.
22. Annie Vinosha, P., et al., *Investigation on elastic, magnetic, optical and electrical impedance properties of dysprosium doped nickel ferrite nanocrystals*. Journal of Nanoscience and Nanotechnology, 2019. **19**(12): p. 8020-8035.
23. Mousavi, M., A. Habibi-Yangjeh, and M. Abitorabi, *Fabrication of novel magnetically separable nanocomposites using graphitic carbon nitride, silver phosphate and silver chloride and their applications in photocatalytic removal of different pollutants using visible-light irradiation*. Journal of colloid and interface science, 2016. **480**: p. 218-231.
24. Du, X. and I.W. Chen, *Ferroelectric thin films of bismuth-containing layered perovskites: part I, Bi₄Ti₃O₁₂*. Journal of the American Ceramic Society, 1998. **81**(12): p. 3253-3259.
25. Jonscher, A., *Universal Relaxation Law Chelsea Dielectric Group*. 1996, London.
26. Jonscher, A.K., *The 'universal' dielectric response*. nature, 1977. **267**(5613): p. 673-679.
27. Ben Taher, Y., et al., *Conductivity study and correlated barrier hopping (CBH) conduction mechanism in diphosphate compound*. Applied Physics A, 2015. **120**: p. 1537-1543.
28. Mahmoud, K., et al., *Dielectric dispersion in lithium–bismuth–borate glasses*. Current Applied Physics, 2011. **11**(1): p. 55-60.
29. Hcini, F., et al., *Effects of sintering temperature on structural, infrared, magnetic and electrical properties of Cd 0.5 Zn 0.5 FeCrO₄ ferrites prepared by sol–gel route*. Journal of Materials Science: Materials in Electronics, 2020. **31**: p. 14986-14997.
30. Elliott, S., *Ac conduction in amorphous chalcogenide and pnictide semiconductors*. Advances in physics, 1987. **36**(2): p. 135-217.
31. Ghosh, A. and A. Pan, *Scaling of the conductivity spectra in ionic glasses: dependence on the structure*. Physical review letters, 2000. **84**(10): p. 2188.
32. Kumari, K., K. Prasad, and R. Choudhary, *Impedance spectroscopy of (Na_{0.5}Bi_{0.5})(Zr_{0.25}Ti_{0.75})O₃ lead-free ceramic*. Journal of alloys and Compounds, 2008. **453**(1-2): p. 325-331.
33. Bruce, P., *High and low frequency Jonscher behaviour of an ionically conducting glass*. Solid State Ionics, 1985. **15**(3): p. 247-251.
34. Elliott, S. and F. Henn, *Application of the Anderson-Stuart model to the AC conduction of ionically conducting materials*. Journal of non-crystalline solids, 1990. **116**(2-3): p. 179-190.
35. Khusayfan, N.M., A. Qasrawi, and H.K. Khanfar, *Design and electrical performance of CdS/Sb₂Te₃ tunneling heterojunction devices*. Materials Research Express, 2018. **5**(2): p. 026303.
36. Long, A., *Frequency-dependent loss in amorphous semiconductors*. Advances in physics, 1982. **31**(5): p. 553-637.
37. Qasrawi, A. and M. Taleb, *Enhancement of electrical performance of ZnSe thin films via Au nanosandwiching*. 2020.
38. Graça, M., et al., *Electrical characterization of SiO₂: LiNbO₃ glass and glass–ceramics using dc conductivity, TSDC measurements and dielectric spectroscopy*. Journal of non-crystalline solids, 2007. **353**(47-51): p. 4390-4394.
39. Ghosh, A., *Frequency-dependent conductivity in bismuth-vanadate glassy semiconductors*. Physical review B, 1990. **41**(3): p. 1479.
40. Behera, C., P.R. Das, and R. Choudhary, *Structural and electrical properties of mechanothermally synthesized NiFe₂O₄ nanoceramics*. Journal of electronic materials, 2014. **43**: p. 3539-3549.
41. Jadhav, S.S., et al., *Structural and electric properties of zinc substituted NiFe₂O₄ nanoparticles prepared by co-precipitation method*. Physica B: Condensed Matter, 2010. **405**(12): p. 2610-2614.
42. Havriliak, S. and S. Negami, *A complex plane representation of dielectric and mechanical relaxation processes in some polymers*. Polymer, 1967. **8**: p. 161-210.

43. Molnár, G., et al., *Interplay between the charge transport phenomena and the charge-transfer phase transition in $Rb_x Mn [Fe(CN)_6]_y \cdot z H_2O$* . The Journal of Physical Chemistry C, 2009. **113**(6): p. 2586-2593.
44. Paul, T. and A. Ghosh, *Dielectric properties of $La_{2-x} Bi_x Mo_2 O_9$ ($0 \leq x \leq 0.4$) ionic conductors*. Materials Research Bulletin, 2014. **59**: p. 416-420.
45. Giuntini, J., et al., *Temperature dependence of dielectric losses in chalcogenide glasses*. Journal of Non-Crystalline Solids, 1981. **45**(1): p. 57-62.
46. Gopalan, E.V., et al., *Evidence for polaron conduction in nanostructured manganese ferrite*. Journal of Physics D: Applied Physics, 2008. **41**(18): p. 185005.
47. Eyring, H., *Viscosity, plasticity*. J. Chem. Phys., 1936. **4**: p. 291.
48. Hcini, F., J. Khelifi, and K. Khirouni, *Enhanced Electrical, Optical and Thermodynamics Properties of $Pr_{0.5} Ce_{0.5} CoO_3$ Cobaltite Prepared Using Sol-Gel Route for Electrical and Optical Applications*. Journal of Inorganic and Organometallic Polymers and Materials, 2023. **33**(10): p. 3178-3194.
49. Pan, K., et al., *Oxygen vacancy mediated surface charge redistribution of Cu-substituted $LaFeO_3$ for degradation of bisphenol A by efficient decomposition of H_2O_2* . Journal of hazardous materials, 2020. **389**: p. 122072.
50. Dutta, V., et al., *Review on augmentation in photocatalytic activity of $CoFe_2O_4$ via heterojunction formation for photocatalysis of organic pollutants in water*. Journal of Saudi Chemical Society, 2019. **23**(8): p. 1119-1136.
51. Yao, Y., et al., *Enhanced photo-Fenton-like process over Z-scheme $CoFe_2O_4/gC_3N_4$ heterostructures under natural indoor light*. Environmental Science and Pollution Research, 2016. **23**: p. 21833-21845.
52. He, H.-Y. and J. Lu, *Highly photocatalytic activities of magnetically separable reduced graphene oxide- $CoFe_2O_4$ hybrid nanostructures in dye photodegradation*. Separation and Purification Technology, 2017. **100**(172): p. 374-381.